

# Mathematical and Numerical Explanation of the Nonlinear Acoustic Wave Interaction in Acousto-Optical Cells

**Abbes Ourahmoun**

Institute of Optics and Precision Mechanics, Ferhat Abbas University, Setif, Algeria  
ourahmounabbes@yahoo.fr (corresponding author)

**Amir Guessoum**

Applied Optics Laboratory, Institute of Optics and Precision Mechanics, Ferhat Abbas University, Setif  
Algeria  
amiroptc@yahoo.fr

Received: 6 July 2024 | Revised: 29 July 2024 and 6 August 2024 | Accepted: 11 August 2024

Licensed under a CC-BY 4.0 license | Copyright (c) by the authors | DOI: <https://doi.org/10.48084/etasr.8315>

## ABSTRACT

In addition to a recently acousto-optical deflector that has been the subject of both theoretical and experimental analysis, this work presents the successful processing of two acousto-optical deflectors that have been orthogonally positioned using two frequency-modulated ultrasonic waves. A comprehensive theoretical analysis is conducted, based on the Collins integral and the ABCD matrix formalism, to explain how the positions of the diffracted orders oscillate in two dimensions as a function of time. The numerical simulation of the derived formula demonstrates the potential for steering a laser beam along Lissajous trajectories. The trajectories in question are observed to exhibit a variety of shapes and velocities. They are sometimes linear with sinusoidal velocities, sometimes circular with constant velocities, and often elliptical with variable velocities. The noteworthy aspect is that all these diffracted orders traverse the spatial domain with an identical sweep frequency, despite the heterogeneity of their trajectories and velocities. Furthermore, these trajectories can be shaped by controlling the phase shift value. This technique can be employed in metrology for rotation measurements based on the Doppler effect. Additionally, it can be used to develop a spatial display that enables tracing Lissajous trajectories, rather than relying on an oscilloscope.

*Keywords-laser beam steering; Lissajous trajectories; acousto-optic deflector; ultrasonic wave*

## I. INTRODUCTION

Although the fundamental principles of Acousto-Optic (AO) diffraction have been well established for some time, there was only a limited number of practical applications prior to the invention of the laser. The necessity for optical devices to control laser beams prompted extensive research on these devices, particularly on Acousto-Optic Deflectors (AODs). Significant advancements have been made in the field of AODs over the past few decades. These devices have been employed in a multitude of applications, including the development of Radio Frequency (RF) spectrum analyzers [1], fringe projectors [2-4], optical tweezers for particle trapping [5-9], and frequency shifters [10, 11]. Furthermore, they were employed to attain high diffraction efficiency and a high deflection angle, which were used in a variety of laser-assisted advanced micro processing technologies, including printing, patterning, and doping [12]. Moreover, AODs have been deployed for the regulation of energy shape [13], the fabrication of a functional device for the spatial and temporal control of laser beams [14],

the stirring and rotation of Bose-Einstein condensates, and the control of the focal position of an optical beam in a three-dimensional space with a rapid and precise methodology [15-17]. The high speed of some AODs enabled the driving of an ultra-short pulsed laser beam [18]. In recent years, the use of Frequency-Modulated (FM) signals to obtain AOD has attracted further attention for a number of reasons. The most significant factor is that the three primary parameters of an AOD, namely scanning frequency, scanning direction, and spatial excursion, can be readily regulated by selecting appropriate values for frequency excursion ( $\Delta f$ ) and modulating signal frequency ( $f_m$ ). Furthermore, the selection of these values was completed with the assistance of a frequency generator, as opposed to being conducted manually, which resulted in a notable alignment between the theoretical and experimental outcomes [19-20]. To corroborate the preceding findings, the performed theoretical investigation, founded upon the Collins integral [21-22], was further elaborated by substituting the plane beam with a Gaussian one and the FM ultrasonic wave with two FM ultrasonic waves propagating in two

perpendicular directions. Subsequently, a numerical simulation of the derived formula was conducted to show the two-dimensional Lissajous trajectories that can be generated by each diffracted order. Ultimately, this numerical simulation is further developed to represent all these trajectories simultaneously in the same space, and to elucidate how the phase shift affects the trajectory of each diffracted order.

In order to explicate the manner by which the diffracted orders can be steered in accordance with Lissajous trajectories, it is first necessary to recall that the interaction between the laser beam and the sinusoidal ultrasonic wave results in a modification of the beam's shape, a phenomenon known as beam shaping. The latter can be controlled by two parameters. The first parameter, designated the Raman–Nath parameter  $\Psi = k_0 L \Delta n$ , is proportional to the ultrasonic pressure and describes the diffraction efficiency. The second parameter is the truncation parameter, denoted by  $\mathfrak{R}$  and defined as the ratio of the laser beam waist to the ultrasonic frequency,  $V/f$ . For example, if we take  $\Psi=1.5$  and  $\mathfrak{R} = 0.3$ , a flat-top beam is obtained when using a sinusoidal ultrasonic wave [23-24] and a convex-concave beam is acquired when utilizing a frequency-modulated ultrasonic wave [25]. If the Raman–Nath parameter is maintained at the same value and  $\mathfrak{R}$  is set to 0.53 [26-28], the intensity of the Gaussian beam is no longer continuous. Instead, it is divided into several diffracted orders that oscillate according to Lissajous trajectories [29].

### II. REPRESENTATION OF TWO-DIMENSIONAL ACOUSTO-OPTICAL INTERACTION

This study proposes the construction of an AOC (1), which will be powered by two chirped acoustic waves (2) generated by two piezoelectric transducers that are positioned orthogonally, as shown in Figure 1. The propagation of these chirped acoustic waves in this medium provides two dynamic phase gratings (3), which accurately represent the interaction of the two chirped waves. The interaction of a Gaussian laser beam (4), incident perpendicularly on the AOC, with these two gratings allows for the splitting of the beam into numerous diffracted orders, which are distributed in a two-dimensional manner. In the focal plane of the converging lens (5), situated immediately behind the AOC, the many diffracted orders can be observed navigating according to different trajectories (6). For example, Geroni lemniscate trajectories are obtained when:  $V_Y = 2V_X, \varphi = \pi/4$ .

### III. REGARDING THEORETICAL BACKGROUND

In this proposal, the application of two electrical FM signals is considered, each feeding an orthogonally-placed piezoelectric transducer. The instantaneous frequency of each signal is given in two directions (x, y) by the following two equations, respectively:

$$f_X(t) = f_X + \Delta f_X \sin(2\pi v_X t + \varphi) \tag{1}$$

$$f_Y(t) = f_Y + \Delta f_Y \sin(2\pi v_Y t) \tag{2}$$

where,  $f_X$  and  $f_Y$  are the carrier frequencies,  $v_X, v_Y$  are the modulating signal pulsations,  $\Delta f_X, \Delta f_Y$  are the frequency excursions, and  $\varphi$  is the phase shift.

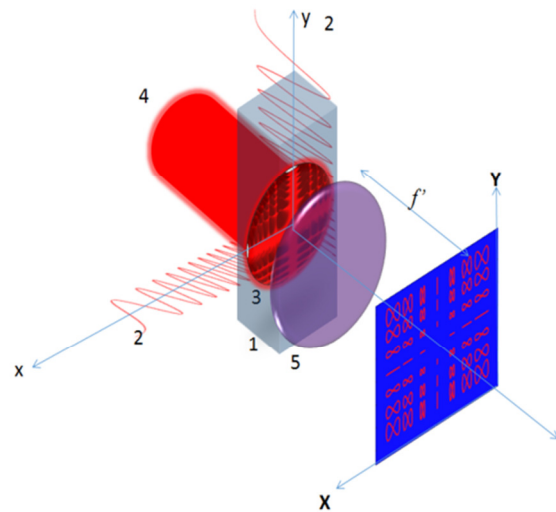


Fig. 1. Schematic representation of two-dimensional acousto-optical interaction.

The traveling ultrasonic waves, generated by these transducers, set up a spatiotemporal modulation of refractive index, which can be described as:

$$n(x, y, t) = n_0 + \Delta n_x \left\{ \sin \left[ \omega_x t - k_x X + \frac{\Delta f_x}{f_m} \sin(2\pi v_x t - k_m X + \varphi) \right] \right\} + \Delta n_y \left\{ \sin \left[ \omega_y t - k_y Y + \frac{\Delta f_y}{f_m} \sin(2\pi v_y t - k_m Y) \right] \right\} \tag{3}$$

where  $n_0$  is the average refractive index of the medium,  $\Delta n_x$  and  $\Delta n_y$  are the index variation amplitude due to the ultrasonic wave in two directions, and  $k_x, k_y, k_m$  are the wave numbers of the carriers and the modulating signal, respectively. In this analysis, a Gaussian laser beam traveling along the z-axis is assumed. The origin ( $z=0$ ) is taken at the meeting point of the two ultrasonic waves, which propagate in perpendicular directions. In order to simplify the subsequent calculations, the constant phase factor will be ignored. In this case, the incident laser beam field can be written as:

$$E(x, y, t) = E_0 \frac{w_0}{w} \exp \left( -\frac{x^2 + y^2}{w^2} \right) \exp(-j\omega t) \tag{4}$$

where  $E_0$  and  $w_0$  are the amplitude and the pulsation of the incident laser beam, respectively, and  $w$  is the beam waist at distance  $z$ . By considering (3) and (4), the output laser beam field is:

$$E_{out}(x, y, t) = E_0 \frac{w_0}{w} \exp \left( -\frac{x^2 + y^2}{w^2} \right) \exp(-j\omega_0 t) \times \exp(-jk_0 L \Delta n_x) \times \left\{ \sin \left[ \omega_x t - k_x x + \frac{\Delta f_x}{f_m} \sin(2\pi v_x t - k_m X + \varphi) \right] \right\} \exp(-jk_0 L \Delta n_y) \left\{ \sin \left[ \omega_y t - k_y y + \frac{\Delta f_y}{f_m} \sin(2\pi v_y t - k_m Y) \right] \right\} \tag{5}$$

Based on the scalar theory of diffraction, the expression of the field at any distance  $z$  along the propagation axis is given by the Collin's integral of diffraction:

$$E(x, y, t) = \frac{j}{\lambda_0 B} \iint_{-\infty}^{+\infty} E_{out}(x, y, t) \exp \left[ \frac{j\pi}{\lambda_0 B} (Ax^2 - 2Xx + DX^2) \right] \exp \left[ \frac{j\pi}{\lambda_0 B} (Ax^2 - 2Xx + DX^2) \right] \quad (6)$$

where  $(x, y)$  are the spatial coordinates for the plane after the optical system defined by the transfer matrix  $ABCD$ . By replacing (5) with (6) we get:

$$E(x, y, z, t) = \frac{j}{\lambda_0 B} E_0 \frac{w_0}{w} \exp(-jw_0 t) \exp(-jk_0 L n_0) \exp \left[ \frac{j\pi}{\lambda_0 B} (DX^2) \right] \exp \left[ \frac{j\pi}{\lambda_0 B} (DY^2) \right] \iint_{-\infty}^{+\infty} \exp(-jk_0 L \Delta n_x \{ \sin[\omega_x t - k_x X + \frac{\Delta f_x}{f_m} \sin(2\pi v_x t - k_m X + \varphi)] \} \exp(-jk_0 L \Delta n_y \{ \sin[\omega_y t - k_y Y + \frac{\Delta f_y}{f_m} \sin(2\pi v_y t - k_m Y)] \} \times \exp \left( -\frac{x^2 + y^2}{w^2} \right) \times \exp \left[ \frac{j\pi}{\lambda_0 B} (Ax^2 - 2Xx) \right] \exp \left[ \frac{j\pi}{\lambda_0 B} (Ay^2 - 2Yy) \right] \quad (7)$$

After a lengthy and arduous calculation, the preceding equation can be reformulated as:

$$I(X, Y) = \left( \frac{\pi E_0 w w_0}{\lambda_0 f'} \right)^2 \sum_{p=-\infty}^{+\infty} [J_p(\psi_x)]^2 \exp \left[ -2 \left( \frac{\pi w}{\lambda_0 f'} X - p\pi \Re_x \left( 1 + \frac{\Delta f_x}{f_x} \cos(2\pi v_x t + \varphi) \right) \right)^2 \right] \sum_{q=-\infty}^{+\infty} [J_q(\psi_y)]^2 \exp \left[ -2 \left( \frac{\pi w}{\lambda_0 f'} Y - q\pi \Re_y \left( 1 + \frac{\Delta f_y}{f_y} \cos(2\pi v_y t + \varphi) \right) \right)^2 \right] \quad (8)$$

where  $\psi_x, \psi_y$  are the Raman-Nath parameters, while  $\Re_x, \Re_y$  are the truncation parameters in two directions.

Equation (8) allows to establish a highly intriguing theoretical framework that elucidates the two-dimensional distribution of diffracted orders when a sinusoidal ultrasonic wave is employed, as well as the periodic oscillation of these orders as a function of time when the ultrasonic wave is frequency-modulated. It is important to highlight that when an ultrasonic wave is sinusoidal with a constant frequency, the resulting formula is identical to that presented in [23-24]. A notable correlation with the theoretical formula is developed in [19], which assumes that a plane wave is presented and the exponent multiplied by the integer number  $p$  or  $q$  indicates that the intensity varies in two dimensions with period  $T_m = \frac{1}{v_x}$ .

#### IV. NUMERICAL SIMULATIONS AND RESULTS

In order to present the position of each diffracted order in two dimensions, the numerical simulation of (8) was conducted. If the identical medium employed in [19-20] is used, which exhibits an ultrasonic velocity of  $V=1,488$  m/s, and if it is considered that  $\lambda_0=632.8$  nm,  $f'=10$  mm, and  $w=160$   $\mu$ m, the numerical simulation yields the curves presented in Figure 2. In the first axis ( $X$ ), the diffracted orders are spaced the same distance  $d_x = \lambda_0 \frac{f' f_x}{v}$ . Equally, the same thing happens

in the second axis ( $Y$ ), where the distance between diffracted orders is  $d_y = \lambda_0 \frac{f' f_y}{v}$ . The diffracted orders of the third axis ( $\xi$ ) are obtained through the interaction of the diffracted orders of the two axes. The direction of this axis and the distance between its diffracted orders ( $d_\xi$ ) are determined, respectively:

$$\phi = \arctan \left( \frac{f_x}{f_y} \right) \quad (9)$$

$$d_\xi = \frac{\lambda_0 f'}{v} \sqrt{f_x^2 + f_y^2} \quad (10)$$

If sinusoidal ultrasonic waves are replaced by frequency-modulated waves with the same frequency excursion ( $\Delta f_x = \Delta f_y = 3$  MHz), the same modulating signal frequency ( $f_x = f_y = 20$  MHz), and  $\varphi = 0$ , the numerical simulation of (8) emerges and is presented in Figures 3 and 4. In theory, the position of each diffracted order oscillates periodically along each axis as a function of time with a scanning frequency of  $f_s$  equal to  $f_m$ . The highest position is reached at  $t=0$ , after which the position gradually decreases until it reaches the lowest position at  $t=T_m/2$ , passing through the medium position obtained at  $t=T_m/4$ . At  $t=T_m$ , the diffracted order returns to the initial position at  $t=0$ . Therefore, it can be deduced that when an FM signal is used, the positions of the diffracted orders are no longer constant as in the first case (Figure 1), but oscillate periodically in three directions. The numerical results corroborate the findings in [19, 20], which were derived from both theoretical and experimental investigations into one-dimensional diffraction. It is important to note that these results can be observed experimentally using two piezoelectric transducers placed orthogonally and having the same resonance frequency, or using a single piezoelectric transducer and an aluminum plate inclined at  $45^\circ$  to reflect the ultrasonic beam, thereby generating an ultrasonic wave that propagates in the  $Y$  direction. In order to avoid the overlapping of diffracted orders, only five values of time have been selected:  $t=0, T_m/4, T_m/2, 3T_m/4,$  and  $T_m$ . The spatial excursion of the diffracted order (1,1) is noted to vary in a linear fashion as a function of frequency excursion:

In the  $X$  axis, the spatial excursion is  $\Delta X$ :

$$\begin{cases} X_{max} = \frac{\lambda_0 f'}{v} (f_x + \Delta f_x) \\ X_{min} = \frac{\lambda_0 f'}{v} (f_x - \Delta f_x) \end{cases} \Rightarrow \Delta X = \frac{X_{max} - X_{min}}{2} \quad (11)$$

In  $\xi$  axis, the spatial excursion is  $\Delta \xi$ :

$$\begin{cases} \xi_{max} = \frac{\lambda_0 f'}{v} \sqrt{(f_x + \Delta f_x)^2 + (f_y + \Delta f_y)^2} \\ \xi_{min} = \frac{\lambda_0 f'}{v} \sqrt{(f_x - \Delta f_x)^2 + (f_y - \Delta f_y)^2} \end{cases} \quad (12)$$

If  $\Delta f_x = \Delta f_y, f_x = f_y$ , the spatial excursion is given by:

$$\begin{cases} \xi_{max} = \frac{\lambda_0 f'}{v} (f_x + \Delta f_x) \sqrt{2} \\ \xi_{min} = \frac{\lambda_0 f'}{v} (f_x - \Delta f_x) \sqrt{2} \end{cases} \Rightarrow \Delta \xi = \frac{\xi_{max} - \xi_{min}}{2} \quad (13)$$

Therefore, it can be concluded that  $\Delta \xi = \Delta X \sqrt{2}$ , which aligns with the numerical values derived from the curves in Figure 3.

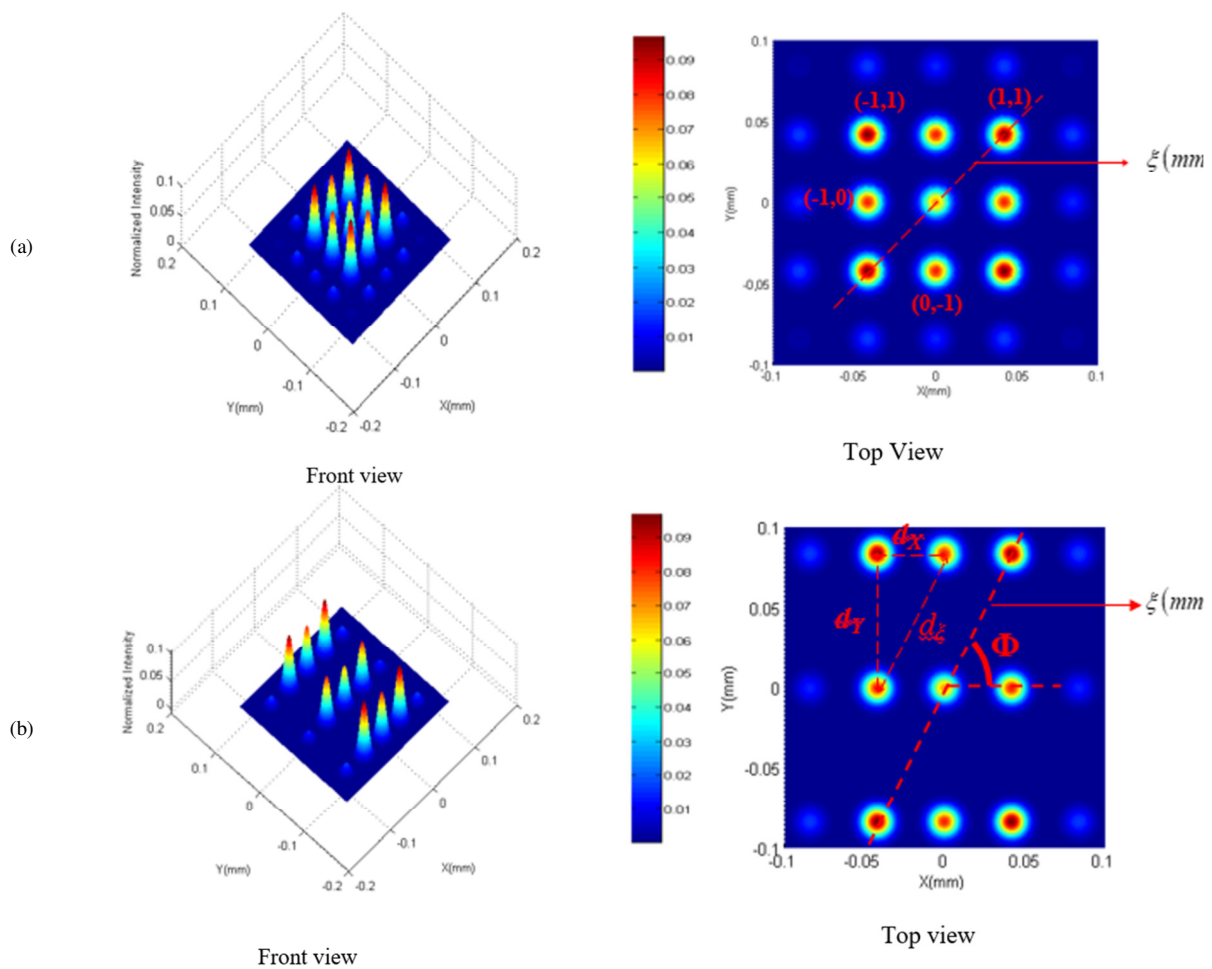


Fig. 2. Representation of intensity two-dimensional distribution of diffracted orders: (a)  $f_x = f_y = 10\text{MHz}$  ( $\phi = 45^\circ$ ), (b)  $f_y = 2f_x = 20\text{ MHz}$ ,  $\phi = 63.43^\circ$ .

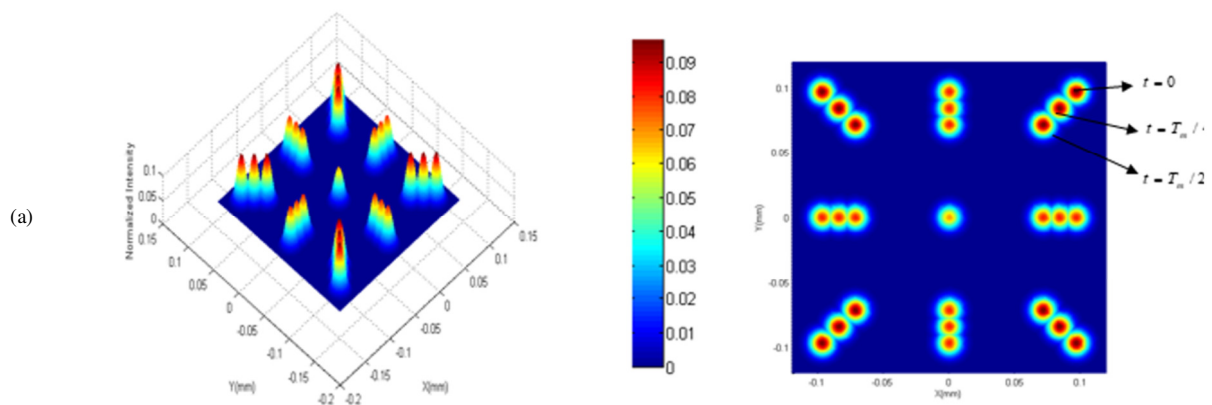


Fig. 3. Representation of intensity two-dimensional distribution of diffracted orders for different values of time, (a) front view, (b) top view.

In addition to the presented linear trajectories, alternative trajectories can be generated by modifying the phase shift value, as portrayed in Figure 5. The objective of this study is to generate all the required trajectories simultaneously and in a single space by increasing the RAMAN-NATH parameter. Figure 6 demonstrates the emergence of higher diffracted orders as the parameter is increased and the impact of phase

shift variation on the trajectory of each diffracted order is augmented.

The numerical simulation of the theoretical formula demonstrates the existence of numerous diffracted orders, some of which oscillate in accordance with linear and simultaneous movements along the two axes (X, Y), while others exhibit

linear, circular, or elliptical motion contingent on the specific shift phase value. When  $\varphi=0^\circ$  or  $\varphi=180^\circ$ , radial and azimuthal linear trajectories are obtained, respectively. When  $\varphi=90^\circ$ , circular, horizontal, and vertical elliptical trajectories are obtained. For the remaining phase shift values, diagonal elliptical trajectories with different slopes are attained. Notably, despite the diversity of trajectories and velocities, all these diffracted orders navigate in space with the same sweep frequency.

steering. This paper presents a theoretical and numerical demonstration of the ability to split an incident laser beam into multiple diffracted orders. Each of the resulting beams travels in space according to its own trajectory and velocity. The linear trajectories are distinguished by a sinusoidal velocity, whereas the circular ones exhibit a constant velocity.

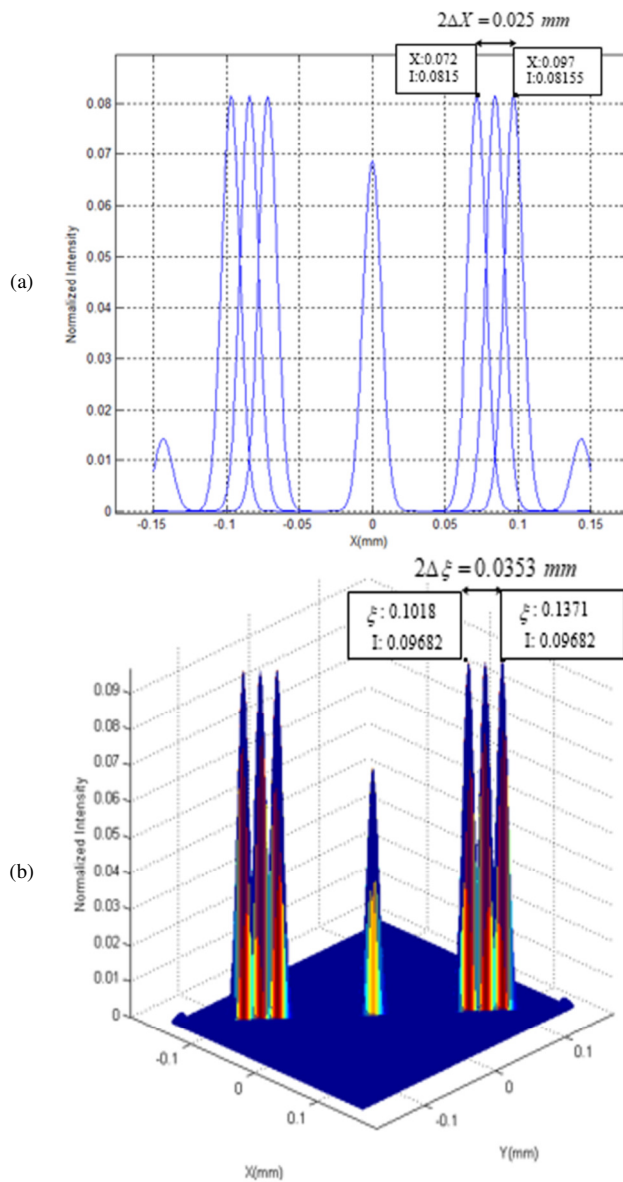


Fig. 4. Representation of intensity one-dimensional distribution of diffracted orders for different values of time.

V. CONCLUSIONS

The interaction of a laser beam with two chirped acoustic waves propagating in two perpendicular directions permitted the development of two distinct fields: beam shaping and beam

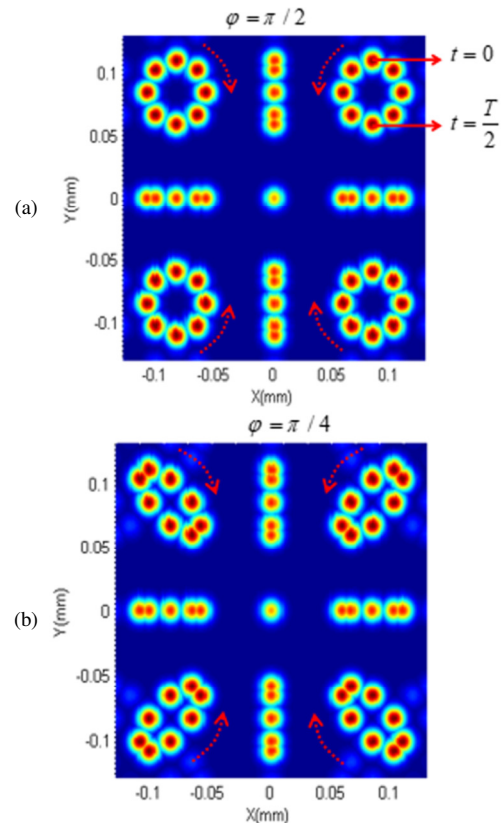


Fig. 5. Representation of intensity two-dimensional distribution of diffracted orders for different values of time:  $t = 0, \frac{T_m}{8}, \frac{2T_m}{8}, \frac{3T_m}{8}, \frac{4T_m}{8}, \frac{5T_m}{8}, \frac{6T_m}{8}, \frac{7T_m}{8}$ , (a)  $\varphi=\pi/2$ , (b)  $\varphi=\pi/4$ .

The derived formulas enabled the enumeration of all key parameters that can influence the shape, velocity, and intensity of the diffracted order. These include phase shift, modulation frequency, frequency amplitudes, Raman-Nath parameters, and more. The purpose of this study was to illustrate that the diffracted order (1,1) can oscillate linearly or elliptically, with varying slopes, contingent on the phase shift and frequency amplitudes. Moreover, the number of diffracted orders is primarily contingent upon the Raman-Nath parameter, whereby an increase in this parameter gives rise to the emergence of high-order diffracted orders. The ability to tune these trajectories at will allow for the generation of an Optical Dynamic Spatial Array (ODSA). The diffracted orders of this ODSA oscillate with the same sweep frequency, which is equal to the modulation frequency  $\nu$ , despite the diversity of trajectories and velocities. It is noteworthy that the presented work remains applicable in the Bragg regime, which is used in numerous applications, including:

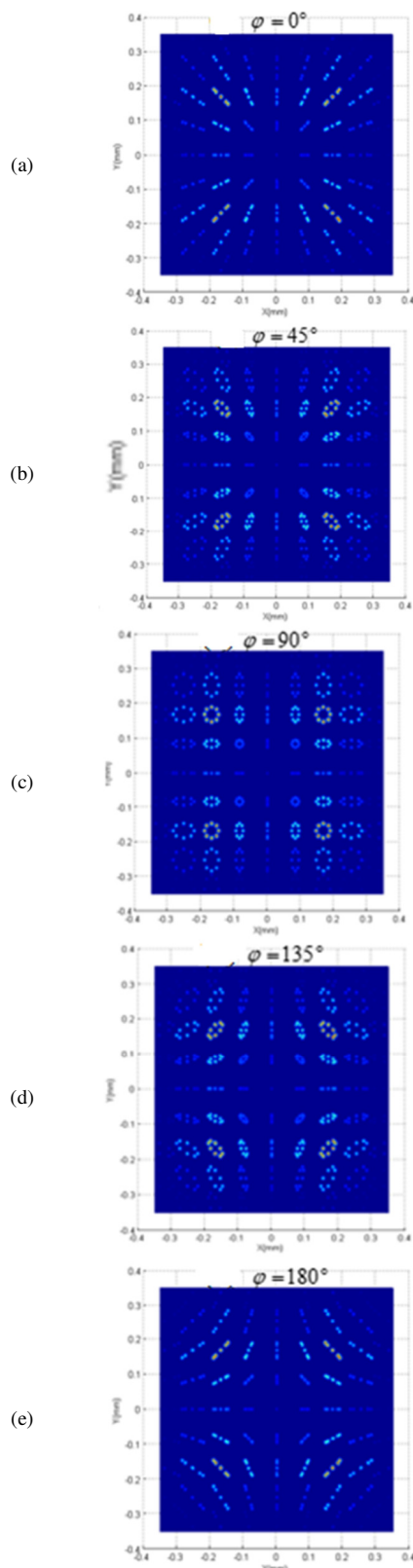


Fig. 6. Representation of intensity two-dimensional distribution of diffracted orders for different values of time and different values of phase shift, (a)  $\varphi=0^\circ$ , (b)  $\varphi=45^\circ$ , (c)  $\varphi=90^\circ$ , (d)  $\varphi=135^\circ$ , (e)  $\varphi=180^\circ$ .

- Generation of a controlled array of spots (matrix of light), wherein the intensity weights of the various diffraction orders may be modified by influencing certain pivotal acousto-optics parameters.
- The generation of laser spots with customized trajectories, speeds, and accelerations. The latter can be employed in metrology for the measurement of rotation (in terms of both speed and acceleration) based on the Doppler effect.
- As an intriguing application, Acousto-Optic Deflector (AOD) can be employed in laser scanners, wherein the diffraction spots are steered to facilitate rapid and precise displacement across any area with high resolution. This is achieved through the use of specific trajectories that are deployed in laser scanners.
- Furthermore, this technique can be employed to develop a spatial display that enables the tracing of Lissajous trajectories, eliminating the necessity for an oscilloscope.

#### REFERENCES

- [1] A. Boulaouad, A. Ourahmoun, and T. Serrar, "Analysis of a Frictionless Electro Viscoelastic Contact Problem with Signorini Conditions," *Engineering, Technology & Applied Science Research*, vol. 12, no. 5, pp. 9224–9228, Oct. 2022, <https://doi.org/10.48084/etasr.5192>.
- [2] S. Dupont, J. C. Kastelik, and F. Causa, "Wide-band acousto-optic deflectors with high efficiency for visible range fringe pattern projector," *Review of Scientific Instruments*, vol. 78, no. 10, Oct. 2007, Art. no. 105102, <https://doi.org/10.1063/1.2793775>.
- [3] S. Dupont and J. C. Kastelik, "Demonstration of a tunable two-frequency projected fringe pattern with acousto-optic deflectors," *The Review of Scientific Instruments*, vol. 79, no. 5, May 2008, Art. no. 056101, <https://doi.org/10.1063/1.2919054>.
- [4] S. H. Dupont, J.-C. Kastelik, and M. Pommeray, "Structured Light Fringe Projection Setup Using Optimized Acousto-Optic Deflectors," *IEEE/ASME Transactions on Mechatronics*, vol. 15, no. 4, pp. 557–560, Aug. 2010, <https://doi.org/10.1109/TMECH.2010.2052627>.
- [5] A. H. Mack, M. K. Trías, and S. G. J. Mochrie, "Precision optical trapping via a programmable direct-digital-synthesis-based controller for acousto-optic deflectors," *The Review of Scientific Instruments*, vol. 80, no. 1, Jan. 2009, Art. no. 016101, <https://doi.org/10.1063/1.3053122>.
- [6] T. Scussiato, W. H. Ito, J. Ramis, and P. I. B. de Queiroz, "A Numerical Model for Heat and Moisture Transfer in Porous Media of Building Envelopes," *Engineering, Technology & Applied Science Research*, vol. 12, no. 5, pp. 9239–9246, Oct. 2022, <https://doi.org/10.48084/etasr.5120>.
- [7] A. E. Wallin, H. Ojala, E. Hægström, and R. Tuma, "Stiffer optical tweezers through real-time feedback control," *Applied Physics Letters*, vol. 92, no. 22, Jun. 2008, Art. no. 224104, <https://doi.org/10.1063/1.2940339>.
- [8] R. V. Brooks *et al.*, "Preparation of one  $87\text{Rb}$  and one  $133\text{Cs}$  atom in a single optical tweezer," *New Journal of Physics*, vol. 23, no. 6, Jun. 2021, Art. no. 065002, <https://doi.org/10.1088/1367-2630/ac0000>.
- [9] Y. Bao *et al.*, "Fast optical transport of ultracold molecules over long distances," *New Journal of Physics*, vol. 24, no. 9, Sep. 2022, Art. no. 093028, <https://doi.org/10.1088/1367-2630/ac900f>.
- [10] A. Guessoum and I. Y. Bouderbala, "Generation of an Optical Spatial Array Oscillating According to Tunable Trajectories and Velocities," *Acoustical Physics*, vol. 70, no. 2, pp. 248–258, Apr. 2024, <https://doi.org/10.1134/S106377102360136X>.
- [11] I. Y. Bouderbala, A. Guessoum, S. Rabhi, O. Bouhlassa, and I.-E. Bouras, "Optical band-diagram, Urbach energy tails associated with photoluminescence emission in defected ZnO thin films deposited by sol-gel process dip-coating: effect of precursor concentration," *Applied Physics A*, vol. 130, no. 3, Feb. 2024, Art. no. 205, <https://doi.org/10.1007/s00339-024-07366-1>.

- [12] T. Wang, C. Zhang, A. Aleksov, I. Salama, and A. Kar, "Effect of large deflection angle on the laser intensity profile produced by acousto-optic deflector scanners in high precision manufacturing," *Journal of Laser Applications*, vol. 28, no. 1, Dec. 2015, Art. no. 012012, <https://doi.org/10.2351/1.4937174>.
- [13] S. N. Antonov and Yu. G. Rezvov, "Acousto-Optic Control of the 2D Energy Profile of Laser Beam," *Technical Physics*, vol. 66, no. 9, pp. 1078–1084, Sep. 2021, <https://doi.org/10.1134/S106378422108003X>.
- [14] Y. V. Pichugina, S. V. Garnov, and Y. N. Bulkin, "2D scanning system of the acousto-optical deflector with high diffraction efficiency," *Journal of Physics: Conference Series*, vol. 2091, no. 1, Nov. 2021, Art. no. 012013, <https://doi.org/10.1088/1742-6596/2091/1/012013>.
- [15] E. R. V. Reddy and S. Thale, "A Novel Efficient Dual-Gate Mixed Dilated Convolution Network for Multi-Scale Pedestrian Detection," *Engineering, Technology & Applied Science Research*, vol. 13, no. 6, pp. 11973–11979, Dec. 2023, <https://doi.org/10.48084/etasr.6340>.
- [16] T. Mamee, W. Anukool, N. Thaicharoen, N. Chattrapiban, and P. Sompert, "Heuristic compactness maximization algorithm for two-dimensional single-atom traps rearrangement," *Journal of Physics: Conference Series*, vol. 2145, no. 1, Dec. 2021, Art. no. 012024, <https://doi.org/10.1088/1742-6596/2145/1/012024>.
- [17] G. J. Evans, P. A. Kirkby, K. M. N. S. Nadella, B. Marin, and R. A. Silver, "Development and application of a ray-based model of light propagation through a spherical acousto-optic lens," *Optics Express*, vol. 23, no. 18, pp. 23493–23510, Sep. 2015, <https://doi.org/10.1364/OE.23.023493>.
- [18] B. K. A. Ngoi, K. Venkatakrishnan, B. Tan, P. Stanley, and L. E. N. Lim, "Angular dispersion compensation for acousto-optic devices used for ultrashort-pulsed laser micromachining," *Optics Express*, vol. 9, no. 4, pp. 200–206, Aug. 2001, <https://doi.org/10.1364/OE.9.000200>.
- [19] A. Guessoum, N. Laouar, and K. Ferria, "Theoretical and experimental study of the light deflection by a frequency modulated ultrasonic wave," *Optics & Laser Technology*, vol. 97, pp. 260–267, Dec. 2017, <https://doi.org/10.1016/j.optlastec.2017.07.002>.
- [20] A. Guessoum, "Scanning Velocity Measurement of an Acousto-Optic Deflector," *Optics and Spectroscopy*, vol. 126, no. 4, pp. 443–449, Apr. 2019, <https://doi.org/10.1134/S0030400X1904009X>.
- [21] S. A. Collins, "Lens-System Diffraction Integral Written in Terms of Matrix Optics," *Journal of the Optical Society of America (JOSA)*, vol. 60, no. 9, pp. 1168–1177, Sep. 1970, <https://doi.org/10.1364/JOSA.60.001168>.
- [22] J. Goodman, *Introduction to Fourier Optics*, 3rd edition. Englewood, Colorado, USA: Roberts and Company Publishers, 2004.
- [23] Y. Ohtsuka, Y. Arima, and Y. Imai, "Acoustooptic 2-D profile shaping of a Gaussian laser beam," *Applied Optics*, vol. 24, no. 17, pp. 2813–2819, Sep. 1985, <https://doi.org/10.1364/AO.24.002813>.
- [24] Y. Ohtsuka and A. Tanone, "Acousto-optic intensity modification of a gaussian laser beam," *Optics Communications*, vol. 39, no. 1, pp. 70–74, Sep. 1981, [https://doi.org/10.1016/0030-4018\(81\)90457-0](https://doi.org/10.1016/0030-4018(81)90457-0).
- [25] A. Guessoum, "Convexity and Concavity Control of Laser Beam Using a Frequency Modulated Acoustic Wave," *Acoustical Physics*, vol. 68, no. 6, pp. 542–548, Dec. 2022, <https://doi.org/10.1134/S1063771022960016>.
- [26] A. Guessoum, "Laser beam Steering According to Linear Trajectories Using an Acousto-Optic Cell," *Acoustical Physics*, vol. 69, no. 1, pp. 53–57, Feb. 2023, <https://doi.org/10.1134/S1063771022600565>.
- [27] A. Guessoum, "Acousto-Optic Scanning of a Laser Beam Along a Reconfigurable Circular Trajectory," *Acoustical Physics*, vol. 69, no. 4, pp. 487–491, Aug. 2023, <https://doi.org/10.1134/S1063771023600183>.
- [28] A. Guessoum and A. Bencheikh, "Laser beam array spot steering customized trajectories using the acousto-optic effect," *Applied Optics*, vol. 62, no. 25, pp. 6585–6592, Sep. 2023, <https://doi.org/10.1364/AO.494636>.
- [29] A. Guessoum and I. Y. Bouderbala, "Spatial representation of Lissajous trajectories by an optical method," *Applied Physics A*, vol. 130, no. 7, Jun. 2024, Art. no. 472, <https://doi.org/10.1007/s00339-024-07615-3>.